

Near-Eye Light Field Displays

Douglas Lanman David Luebke
NVIDIA Research

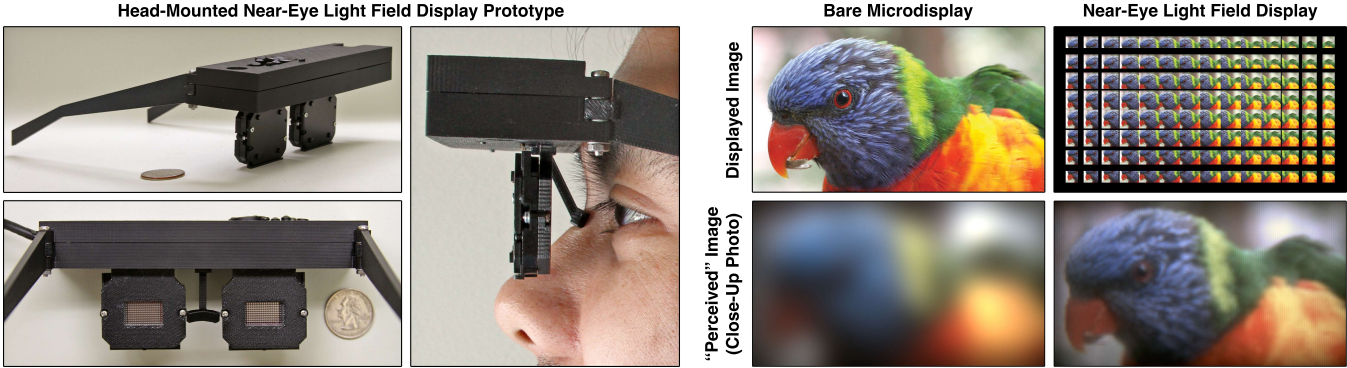


Figure 1: Enabling thin, lightweight near-eye displays using light field displays. (Left) Our binocular near-eye display prototype is shown, comprising a pair of OLED panels covered with microlens arrays. This design enables a thin head-mounted display, since the black box containing driver electronics could be waist-mounted with longer OLED ribbon cables. (Right) Due to the limited range of human accommodation, a severely defocused image is perceived when a bare microdisplay is held close to the eye. Conventional near-eye displays require bulky magnifying optics to facilitate accommodation. We propose near-eye light field displays as thin, lightweight alternatives, achieving comfortable viewing by synthesizing a light field for a virtual scene located within the accommodation range (here implemented by viewing a microdisplay, depicting interlaced perspectives, through a microlens array). Lorikeet source image courtesy of Robyn Jay.

Abstract

We propose near-eye light field displays that enable thin, lightweight head-mounted displays (HMDs) capable of presenting nearly correct convergence, accommodation, binocular disparity, and retinal defocus depth cues. Sharp images are depicted by out-of-focus elements by synthesizing light fields corresponding to virtual objects within a viewer’s natural accommodation range. We formally assess the capabilities of microlens arrays to achieve practical near-eye light field displays. Building on concepts shared with existing integral imaging displays and light field cameras, we optimize performance in the context of near-eye viewing. We establish fundamental trade-offs between the quantitative parameters of resolution, field of view, and depth of field, as well as the ergonomic parameters of form factor and ranges of allowed eye movement. As with light field cameras, our design supports continuous accommodation of the eye throughout a finite depth of field; as a result, binocular configurations provide a means to address the accommodation-convergence conflict occurring with existing stereoscopic displays. We construct a complete prototype display system, comprising: a custom-fabricated HMD using modified off-the-shelf parts and real-time, GPU-accelerated light field renderers (including a general ray tracing method and a “backward compatible” rasterization method supporting existing stereoscopic content). Through simulations and experiments, we motivate near-eye light field displays as thin, lightweight alternatives to conventional near-eye displays.

Links: [DL](#) [PDF](#) [WEB](#) [VIDEO](#)

CR Categories: B.4.2 [Input/Output and Data Communications]: Input/Output Devices—Image Display I.3.7 [Computer Graphics]: Three-Dimensional Graphics and Realism—Virtual Reality

Keywords: light field displays, head-mounted displays, microlens arrays, accommodation-convergence conflict, virtual reality

1 Introduction

Near-eye displays project images directly into a viewer’s eye, encompassing both head-mounted displays (HMDs) and electronic viewfinders. Such displays confront a fundamental problem: the unaided human eye cannot accommodate (focus) on objects placed in close proximity (see Figure 1). As reviewed by Rolland and Hua [2005], a multitude of optical solutions have been proposed since Sutherland [1968] introduced the first graphics-driven HMD. The majority of such designs emulate the behavior of a simple magnifier: synthesizing an enlarged image of a miniaturized display, appearing to be located within the viewer’s natural accommodation range. To be of practical utility, a near-eye display should provide high-resolution, wide-field-of-view imagery with compact, comfortable magnifying optics. However, current magnifier designs typically require multiple optical elements to minimize aberrations, leading to bulky eyewear with limited fields of view that have, to date, prohibited widespread consumer adoption.

Conventional displays are intended to emit light isotropically. In contrast, a light field display supports the control of tightly-clustered bundles of light rays, modulating radiance as a function of position and direction across its surface. We consider a simple near-eye architecture: placing a light field display directly in front of a user’s eye (or a pair of such displays for binocular viewing). As shown in Figure 1, sharp imagery is depicted by synthesizing a light field for a virtual display (or a general 3D scene) within the viewer’s unaided accommodation range. As characterized in this paper, near-eye light field displays provide a means to achieve thin, lightweight HMDs with wide fields of view and to address accommodation-convergence conflict in binocular configurations; however, these benefits come at a cost: spatial resolution is significantly reduced with microlens-based designs, although with com-

mensurate gains in depth of field and in accurate rendering of retinal defocus blur. It is our goal to assess the viability of this trade-off, in light of: fundamental design limitations, anticipated reductions in microdisplay pixel pitches, manufacturing advantages unique to our proposed display architecture, and the emerging demand for comfortable, yet immersive, HMDs.

1.1 Contributions

Our primary technical contributions are:

- We motivate near-eye light field displays capable of synthesizing sharp images of virtual 3D objects located within a viewer’s natural accommodation range, despite being in close proximity to the eye. We demonstrate such displays are ideally suited for thin-form-factor, wide-field-of-view HMDs.
- We evaluate the capability of microlens arrays to create practical near-eye light field displays. Through a first-order optical analysis, we establish fundamental trade-offs between design parameters, including: form factor, spatial resolution, field of view, depth of field, and retinal blur. We also propose computational microdisplay defect correction methods, unique to our architecture, to improve microdisplay manufacturing yield.
- We demonstrate a complete prototype display system, including a custom-fabricated HMD using modified off-the-shelf parts. We also implement two real-time light field renderers: a GPU-accelerated ray tracer and a “backward compatible” fragment shader supporting existing stereoscopic content.

1.2 Overview of Benefits and Limitations

The primary benefits of near-eye light field displays are reduced thickness and weight (e.g., as achieved by substituting a compact microlens array for compound magnifying optics). Such displays also approximate retinal defocus blur and, correspondingly, offer a means to address accommodation-convergence conflict with binocular configurations. As demonstrated in the supplementary video, our design can also correct for the viewer’s optical aberrations (i.e., their eyeglasses prescription), utilizing the approach of Pamplona et al. [2012] in a near-eye configuration—further establishing a compact, flexible design alternative.

The primary limitation of near-eye light field displays is reduced spatial resolution, which we demonstrate is proportional to the ratio of the microlens focal length to the distance of the display from the eye. This creates a fundamental tension between thinner form factors and higher resolutions (without increasing microdisplay pixel pitch). Practical applications will necessitate manufacturing larger microdisplays with smaller pixel pitches, enabling wide fields of view and high resolutions, respectively. (As discussed in Section 5, redundancy within displayed light fields can be exploited to correct manufacturing defects and improve yield.) Microlenses introduce scattering, absorption, and aberrations, particularly at the lens interfaces. Rendering overhead is also increased, however certain approximations minimize this overhead, as described in Section 4.

2 Related Work

2.1 Head-Mounted Displays

While near-eye displays include electronic viewfinders, our primary interest is in facilitating head-mounted, immersive virtual reality (VR). A historical survey of HMDs is presented by Rolland and Hua [2005]. Commercial interest in HMDs has increased with the announcement of Google Glass¹ and the Oculus Rift². The former

is restricted to a narrow field of view located at the periphery of a viewer’s visual field, constituting the first commercial variant of the “digital eye glasses” pioneered by Mann [2012]. Similar to Olson et al. [2011], the latter leverages smartphone technology to provide an immersive, affordable HMD, although with cumbersome headgear.

We are not the first to propose incorporating magnifier arrays within HMDs. Shaoulov et al. [2004] describe the magnification properties for stacks of two dissimilar microlens arrays. Similarly, Urey and Powell [2005] apply dual-microlens arrays as exit-pupil expanders for retinal scanning displays. In a closely related work, Massof et al. [2003] achieve a 150×100 degree binocular field of view using a spherical array of microdisplays viewed through a curved, multi-faceted lens array—a design now commercialized by Sensics, Inc. We emphasize that tiled HMDs are encompassed by our analysis; however, we introduce their use as light field displays, rather than as field-of-view expanders, characterizing their ability to address accommodation-convergence conflict and correct for user’s optical aberrations when applied in denser, thinner arrays to a single microdisplay (i.e., by viewing each microdisplay through a magnifier array, rather than a single magnifier).

2.2 Microlens Array Imaging

Imaging devices routinely incorporate microlens arrays. Anderson [1979] creates a unit magnification relay system using a pair of identical microlens arrays. The first array forms demagnified, inverted images in an intermediate plane; the second is positioned to form erect, partially-overlapping images of this plane, yielding unit magnification. Dispensing with the first array, Hutley et al. [1994] introduce *moiré magnification*: forming a magnified, periodic image when viewing an array of identical objects through a microlens array with a similar period. We recognize near-eye light field displays exploit a related phenomenon; however, the underlying imagery is aperiodic and forms magnified views corresponding to general 3D scenes, rather than periodic planar objects.

Near-eye light field displays share many limitations and benefits with light field cameras. Our microlens-based design is based on the integral imaging method introduced by Lippmann [1908]. By capturing a photograph through a microlens array, an interlaced set of elemental images is recorded, corresponding to a series of off-axis perspective projections. As characterized by Jin et al. [2004], integral imaging mirrors many of the properties of our near-eye display: extending depth of field and field of view, at the cost of decreased spatial resolution. Similar trade-offs are characterized by Ng et al. [2005] for their hand-held light field camera, now commercialized by Lytro, Inc. We emphasize that a key benefit of light field cameras is to allow post-capture *refocusing*; equivalently, near-eye light fields support *focusing* of the eye, with the retina performing a similar integration of optically-aligned, but differing, views.

2.3 3D Displays

Most existing stereoscopic displays suffer from *accommodation-convergence conflict*: presenting accurate binocular disparity (supporting convergence on any point), but only allowing the viewer to accommodate on the display surface. As a result, content is restricted to a “zone of comfort” close to the surface, mitigating accommodation-convergence conflict. However, as characterized by Held et al. [2012], estimation of depth from binocular disparity is accurate near the plane of fixation, whereas retinal blur is more precise elsewhere (i.e., estimating depth from defocus). For near-eye applications, our microlens-based display depicts approximately-correct retinal blur via “super multiview” imagery [Takaki 2006], in which disparity cues are depicted *across a single pupil*.

¹<http://g.co/projectglass> ²<http://www.oculusvr.com>

Near-eye light field displays are not the only means to address accommodation-convergence conflict. Akeley et al. [2004] introduce a multifocal display, rendering images across multiple semi-transparent planes. Rolland et al. [2000] describe a related multi-layer HMD architecture. Rather than requiring multiple physical displays, Love et al. [2009] synthesize a virtual multifocal display using a fast switchable lens synchronized with a single display. Liu et al. [2010] demonstrate addressable focus cues by introducing a liquid lens into a conventional stereoscopic HMD. While such architectures provide near-correct accommodation cues, their construction currently prohibits thin-form-factor HMDs.

Integral imaging displays have previously been applied to estimate and correct viewer's optical aberrations. Pamplona et al. [2010] use near-eye microlens arrays to estimate refractive errors, whereas Pamplona et al. [2012] use integral imaging displays, far from the eye, to correct optical aberrations. We recognize similar methods can be applied with our prototype, mitigating the need for corrective eyewear. In comparison to these closely-related works, we emphasize that this paper differs in scope; we target general-purpose 3D display, rather than estimation and correction of aberrations. Furthermore, we are the first to formally characterize and demonstrate fundamental design trade-offs, optimal optical configurations, and detailed image formation models for virtual reality applications.

Light field displays enable autostereoscopic (glasses-free) 3D viewing. Conventional designs include parallax barriers [Ives 1903] and integral imaging [Lippmann 1908]. We observe many existing light field display technologies may be similarly transformed for near-eye viewing. However, adapting parallax barriers will require addressing limited brightness, visual artifacts, and resolution limitations imposed by diffraction. Some of these limitations may be addressed through time-multiplexed parallax barriers [Kim et al. 2007], eye tracking [Perlin et al. 2000], or multilayer light field displays [Gotoda 2010; Holroyd et al. 2011; Wetzstein et al. 2012]. Regardless of the optical hardware, any near-eye light field display must be paired with an anti-aliasing method [Zwicker et al. 2006].

3 Designing Near-Eye Light Field Displays

This section describes the construction of near-eye light field displays using an array of simple magnifying lenses. Each element is approximated as a thin lens, allowing the derivation of fundamental trade-offs between design parameters and revealing optimal display configurations. Section 3.1 describes the design of a conventional HMD using a simple magnifier to depict a single virtual plane. Section 3.2 analyzes HMDs that employ an array of simple magnifiers to display a single plane. Section 3.3 assesses the degree to which magnifier arrays can be employed as near-eye light field displays, depicting general 3D scenes, to provide approximate accommodation cues within the depth of field supported by each lens element.

3.1 Simple Magnifiers

Consider the following HMD design: a single converging lens, of focal length f and width w_l , is placed a distance $0 < d_l \leq f$ in front of a microdisplay of width w_s and pixel pitch p . As shown in Figure 2, the lens acts as a *simple magnifier* to produce a virtual, erect image of the microdisplay. In practice, the designer specifies the desired distance $d_o \geq 0$ to the virtual image to ensure comfortable accommodation by the viewer. The lens separation d_l is found by applying the Gaussian thin lens formula, as follows.

$$\frac{1}{f} = \frac{1}{d_l} - \frac{1}{d_o - d_e} \Leftrightarrow d_l = \frac{f(d_o - d_e)}{f + (d_o - d_e)}, \text{ for } 0 < d_l \leq f \quad (1)$$

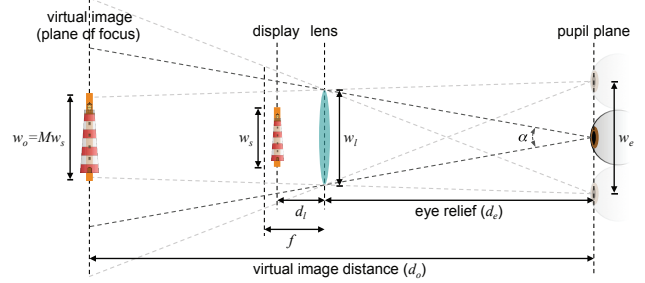


Figure 2: Designing a near-eye display using a simple magnifier. A lens of focal length f and width w_l is positioned a distance d_l in front of a microdisplay of width w_s , creating a magnified virtual image located a distance d_o from the eye. For an eye relief d_e , this design supports an eye box of width w_e , as given by Equation 5.

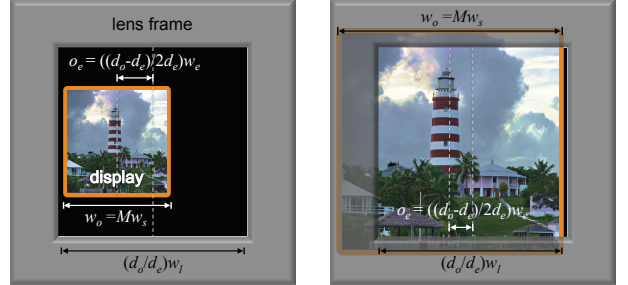


Figure 3: Comparing display-limited and lens-limited simple magnifiers. (Left) A display-limited magnifier, as it appears when viewed from the left-hand side of the eye box. (Right) A lens-limited magnifier viewed from the left-hand side of the eye box. Labels correspond to dimensions projected into the virtual image plane, separated by a distance d_o from the eye. Dashed lines denote the centers of the display and lens, appearing displaced to the viewer by a distance o_e . Lighthouse source image courtesy Bruce Tuten.

Note that the *eye relief* d_e quantifies the separation between the magnifying lens and the viewer's eye. For this configuration, the microdisplay appears magnified by a factor of M , given by

$$M = \frac{w_o}{w_s} = \frac{d_o - d_e}{d_l} = 1 + \left(\frac{d_o - d_e}{f} \right). \quad (2)$$

As shown in Figure 2, the field of view α is defined as the angle subtended by the visible portion of the virtual image, as observed from the viewer's perspective. We distinguish between two possibilities in Figure 3: either the field of view is limited by the dimensions of the magnified microdisplay (shown on the left), or it is limited by the extent of the lens (shown on the right); we refer to the former configuration as a *display-limited magnifier* and to the latter as a *lens-limited magnifier*. Thus, the field of view can be quantified by the following expression.

$$\alpha = 2 \arctan \left[\min \left(\frac{w_l}{2d_e}, \frac{Mw_s}{2d_o} \right) \right] \quad (3)$$

We define the spatial resolution N_p as the number of (magnified) pixels appearing to span the field of view, such that

$$N_p = \left\lfloor \frac{2d_o \tan(\alpha/2)}{Mp} \right\rfloor = \min \left(\left\lfloor \frac{d_o w_l}{de Mp} \right\rfloor, \left\lfloor \frac{w_s}{p} \right\rfloor \right). \quad (4)$$

Equations 3 and 4 can be used to assess the two-dimensional design tradespace, parameterized by the lens focal length f and width w_l , as plotted on the left-hand sides of Figures 5 and 6. We observe

that display-limited magnifiers provide a practical HMD architecture, achieving full-resolution magnified images (i.e., equal to the native microdisplay resolution), although with long focal lengths and wide lenses (i.e., thick, bulky form factors). In contrast, lens-limited magnifiers have limited practical utility, achieving similar fields of view with thinner, narrower optics, but at the cost of reduced resolution and the introduction of vignetting. This trade-off is apparent on the right-hand side of Figure 3, with lens-limited magnifiers only rendering a portion of the microdisplay visible from any given vantage point. However, Section 3.2 reveals that arrays of lens-limited magnifiers have several beneficial properties.

The utility of an HMD not only depends on quantitative measures of resolution and field of view, but also on qualitative judgements of how comfortable it is to wear. We can formally assess these ergonomic factors by deriving constraints on the eye relief d_e , eye box width w_e , and lens focal length f . We observe that simple magnifiers create a *non-pupil-forming* HMD; as shown in Figure 2, the viewer will see the full extent of the virtual image if his pupil is located within the *eye box* of width w_e , oriented parallel to the display surface and displaced by the eye relief d_e .

Figure 3 illustrates the case for which the pupil is located at the left-most extent of the eye box. For display-limited magnifiers, this situation corresponds to the left-hand side of the magnified microdisplay appearing adjacent to the left-hand side of the lens frame. In contrast, for lens-limited magnifiers, the right-hand side of the microdisplay will appear adjacent to the right-hand side of the lens frame. In both cases, the microdisplay center will appear displaced from the lens center by a distance o_e . Thus, the following expression quantifies the maximum-allowable eye box width w_e , such that

$$w_e = \left| \left(\frac{d_o}{d_o - d_e} \right) w_l - \left(\frac{d_e}{d_l} \right) w_s \right|. \quad (5)$$

Unlike pupil-forming HMDs, simple magnifiers allow the viewer to be anywhere in front of the display (within the eye box); however, the eye box width w_e depends on the eye relief d_e , limiting the viewing zone. Wide eye boxes increase comfort, placing fewer constraints on the eyepiece position and allowing binocular designs without requiring manual interpupillary distance (IPD) adjustment.

As presented in Appendix A, the preceding expressions provide a lower bound on the thickness of any HMD using a simple magnifier; this reflects a practical observation: existing magnifier-based HMDs have not yet achieved lightweight, eyeglasses-like form factors, despite decades of development [Kress and Starner 2013].

3.2 Magnifier Arrays

Following Section 1, we propose the following HMD design: a thin, two-dimensional array of converging lenses placed in front of a microdisplay. While conceptually similar to conventional light field displays, particularly integral imaging architectures, the optical configuration and underlying imagery must be optimized for near-eye viewing. We identify that such designs are well characterized for HMD applications by interpreting their construction from a simple perspective: as an array of lens-limited simple magnifiers.

As shown in Figure 4, an array of N_l lenses, each of focal length f and width w_l , is placed a distance d_l in front of a microdisplay. The microdisplay is segmented into *elemental image regions* of width Δw_s . Each region and corresponding lens acts as an independent lens-limited magnifier, synthesizing an off-axis perspective projection of the virtual image plane located a distance d_o from the eye, following Equation 1. Each perspective spans the eye box and has a center of projection coincident with the lens center. Thus, the

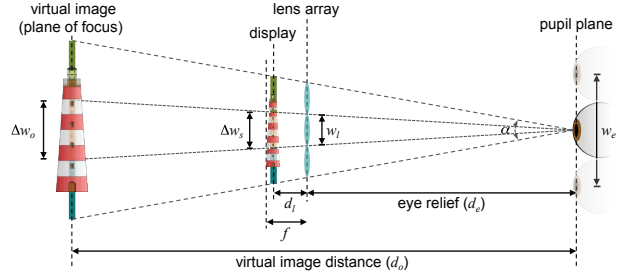


Figure 4: Designing a near-eye display using a magnifier array. An array of N_l lenses, each of focal length f and width w_l , is positioned a distance d_l in front of a microdisplay of width w_s and pixel pitch p . The microdisplay is segmented into regions of width Δw_s , given by Equation 6. Following Section 3.3, a light field is emitted corresponding to a virtual image located a distance d_o from the eye. For an eye relief d_e , this design yields an image with N_p pixels and an eye box of width w_e , given by Equations 8 and 9, respectively.

elemental image width Δw_s is given by

$$\Delta w_s = \min \left[\left(\frac{d_e + d_l}{d_e} \right) w_l, w_s \right], \text{ such that } N_l = \left\lfloor \frac{w_s}{\Delta w_s} \right\rfloor. \quad (6)$$

Only the central microdisplay segment of width $N_l \Delta w_s \leq w_s$ is used with magnifier arrays, avoiding artifacts due to rendering a portion of the virtual image plane visible through peripheral lenses. (This unused periphery ultimately proves useful for correcting alignment errors and optical aberrations in Section 4.) Similarly, the elemental image width Δw_s cannot exceed that of the microdisplay (defaulting to a simple magnifier in this case).

By interpreting a magnifier array as a set of independent lens-limited magnifiers, expressions quantifying field of view α , spatial resolution N_p , and eye box width w_e follow directly from those in Section 3.1. For example, the field of view α is given by

$$\alpha = 2 \arctan \left[\min \left(\frac{N_l w_l}{2 d_e}, \frac{M w_s}{2 d_o} \right) \right], \quad (7)$$

found by substituting the lens array width $N_l w_l$ for the lens width w_l in Equation 3. We emphasize that the first argument of the minimum function applies with magnifier arrays and lens-limited magnifiers, whereas the second argument describes display-limited magnifiers. Similarly, the spatial resolution is given by substituting this field of view for that appearing in Equation 4, as follows.

$$N_p = \left\lfloor \frac{2 d_o \tan(\alpha/2)}{M p} \right\rfloor = \min \left(\left\lfloor \frac{d_o N_l w_l}{d_e M p} \right\rfloor, \left\lfloor \frac{w_s}{p} \right\rfloor \right) \quad (8)$$

The eye box width w_e is determined by that of a single magnifying element. Substituting the elemental image width Δw_s for the microdisplay width w_s in Equation 5 gives the following:

$$w_e = \left| \left(\frac{d_o}{d_o - d_e} \right) w_l - \left(\frac{d_e}{d_l} \right) \Delta w_s \right|. \quad (9)$$

An HMD must support variations in eye position, eye rotation, and pupil diameter; all such variations are tolerated by near-eye light field displays based on magnifier arrays, so long as the pupil remains within a single viewing zone created by the magnifier array. Following Dodgson [2002], the central viewing zone for any multiview display is a 3D volume. The width of this zone, evaluated at the eye relief d_e , corresponds to the eye box width w_e .

Equations 7–9 are evaluated in Figures 5 and 6, charting the design tradespace for magnifier arrays and simple magnifiers. As with

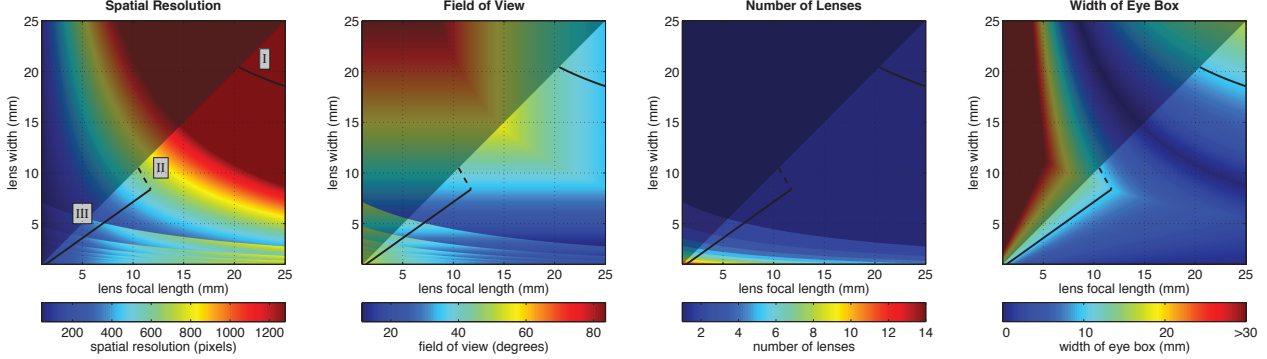


Figure 5: Near-eye display design tradespace. A near-eye display consists of a microdisplay covered by either a simple magnifier or a magnifier array, following Sections 3.1 and 3.2. Key design parameters are evaluated as a function of lens focal length f and width w_l . The microdisplay width $w_s = 15.36$ mm and pixel pitch $p = 12 \mu\text{m}$ correspond to the prototype in Section 4. Spatial resolution, shown on the left, is evaluated for a virtual plane located at a distance $d_o = 1.0$ m. It is impractical to manufacture a lens with a focal length significantly less than its width; this “infeasible” design space is denoted by the shaded region in the upper left of each plot (here assuming an f-number limit of 1.0 such that $f \geq w_l$). Black lines indicate magnifier designs yielding an eye box width $w_e = 10$ mm for an eye relief $d_e = 14$ mm. Labeled regions I, II, and III correspond to display-limited simple magnifiers, lens-limited simple magnifiers, and magnifier arrays, respectively.

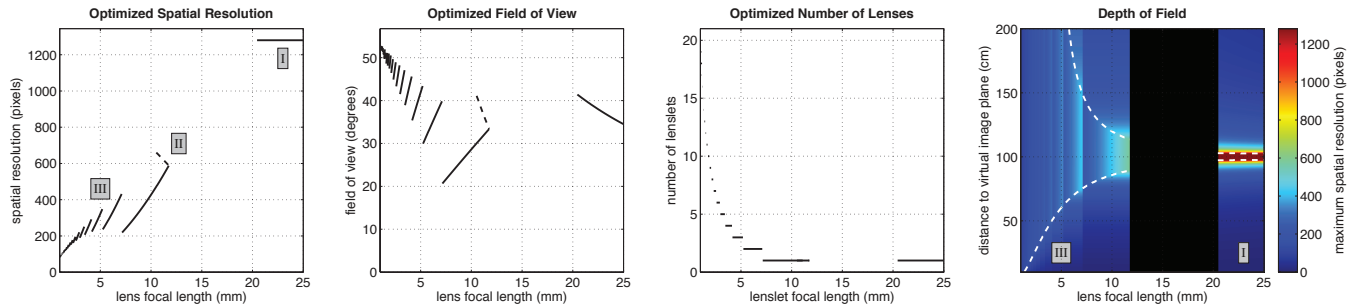


Figure 6: Optimizing near-eye displays. The three figures on the left tabulate key design parameters for simple magnifiers and magnifier arrays yielding an eye box width $w_e = 10$ mm for an eye relief $d_e = 14$ mm, optimized for viewing at a distance $d_o = 1.0$ m. Values are determined by interpolating along the corresponding black lines in Figure 5. The depth of field for the optimized magnifier designs is assessed on the right, as a function of the lens focal length f and the distance to the virtual image plane d'_o , following Equation 13. White lines denote the depth of field: the range of object distances supporting the maximum resolution afforded by the magnifier design, given by Equation 8.

prior tiled HMD designs [Massof et al. 2003], magnifier arrays expand the field of view α by a factor of N_l , without increasing the lens focal length f (or the HMD thickness), assuming the microdisplay width w_s is increased by a proportional factor. Unlike prior tiled HMDs, our construction allows for thinner, planar constructions using a single microdisplay. However, as depicted in Figures 1 and 4, portions of the target image are repeated across the elemental images; as with light field cameras, such repetition reduces the perceived spatial resolution, although with a commensurate gain in accommodation and retinal blur cues, as discussed in Section 3.3.

It is necessary to quantify the “resolution loss” imposed by magnifier arrays to determine their practical utility. We consider the circumstance for which the virtual image is placed at “optical infinity” (i.e., $d_o \gg d_e$). Equation 8 takes the following form:

$$\lim_{d_o \rightarrow \infty} N_p = \left\lfloor \left(\frac{f}{d_e} \right) \left(\frac{N_l w_l}{p} \right) \right\rfloor, \text{ for } w_l \leq \frac{d_e w_s}{d_e + f} \text{ and } d_l = f. \quad (10)$$

The inequality is a necessary condition for a magnifier array, otherwise the elemental image width Δw_s exceeds the microdisplay width w_s , reverting to the case of a simple magnifier. Substituting Equation 6, with the condition $N_l \leq w_s / \Delta w_s$, yields an upper bound on the resolution of magnifier arrays:

$$\lim_{d_o \rightarrow \infty} N_p \leq \left(\frac{f}{d_e + f} \right) \left(\frac{w_s}{p} \right), \text{ for } w_l \leq \frac{d_e w_s}{d_e + f} \text{ and } d_l = f. \quad (11)$$

Equation 11 provides a succinct answer to the question of resolution

loss: **virtual image resolution is reduced, relative to the native microdisplay resolution, by a factor proportional to the ratio of the lens focal length f to the sum of the eye relief d_e and the lens focal length.** Thus, magnifier arrays constitute a new HMD design template that trades microdisplay resolution for thinner form factors and wider fields of view—breaking the fundamental limits imposed by simple magnifiers, as quantified by Equation 19 in Appendix A.

3.3 Near-Eye Light Field Display with Magnifier Arrays

To this point, we have only analyzed the synthesis of a single virtual image plane. However, light field displays are routinely used to depict virtual 3D scenes extending throughout a limited depth of field centered on the display surface. However, we emphasize that the depth of field for near-eye light field displays must be centered *far from the display surface* (i.e., within the human accommodation range). Fortunately, as shown on the right-hand side of Figure 6, this proves to be the case for HMDs using magnifier arrays.

Assume a magnifier array has been optimized following the principles outlined in Section 3.2. As such, the lens separation d_l is fixed via Equation 1 to synthesize a sharp virtual image for an object located at a distance d_o from the eye. When the eye focuses through the lens on an object at a distance $d'_o \neq d_o$, the image will be blurred by a *circle of confusion* of width c'_o , given by

$$c'_o = \max \left[\left(\frac{|d'_o - d_o|}{d_o - d_e} \right) w_l, \left(\frac{d'_o - d_e}{d_l} \right) p \right]. \quad (12)$$

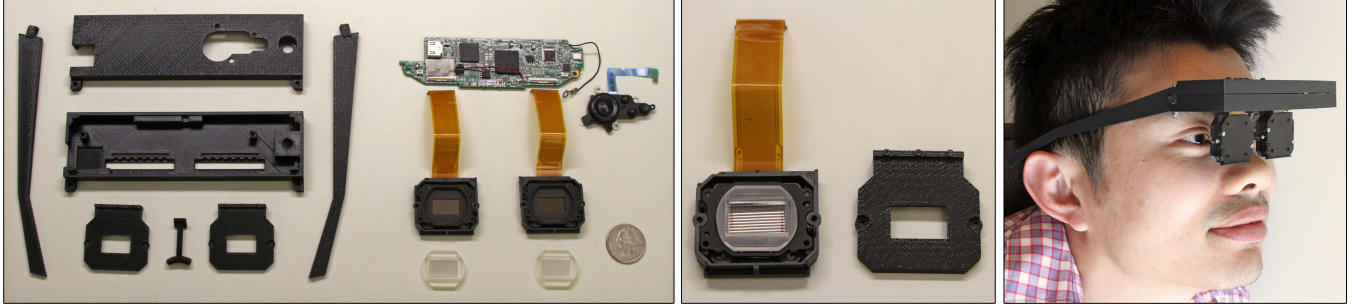


Figure 7: Constructing a near-eye light field HMD. (Left) A custom head-mounted enclosure, comprising the plastic parts shown on the left, was fabricated to hold the Sony HMZ-T1 driver electronics and our modified eyepieces, shown on the right. (Middle) Each modified eyepiece contains a Fresnel Technologies #630 microlens array, mounted in front of a Sony ECX332A OLED microdisplay. (Right) A user wearing the assembled HMD. (See Appendix A of the supplementary material for an extended discussion of the prototype construction.)

The first term corresponds to the depth of field for a thin lens [Goodman 2004], whereas the second term specifies that the blur cannot be less than the pixel pitch p , projected into the plane at d'_o .

The depth of field characterizes the maximum spatial resolution N'_p for a virtual image plane located a distance d'_o from the eye. Similar to Equations 4 and 8, this expression is given by dividing the apparent virtual image extent by the width of the circle of confusion:

$$N'_p = \left\lfloor \frac{2d'_o \tan(\alpha/2)}{c'_o} \right\rfloor, \quad (13)$$

where the field of view α is given by Equation 7. As plotted on the right of Figure 6, the extent of the “high-resolution” portion of the depth of field (i.e., the range of distances d'_o for which Equations 8 and 13 are approximately equal for $\{d_o, d'_o\} \gg d_e$) increases as the lens focal length decreases; for this example, the depth of field supports the four-diopter accommodation range for an average 40-year-old individual (i.e., $d'_o \geq 25$ cm) [Wandell 1995].

Most existing stereoscopic displays suffer from accommodation-convergence conflict (see Section 2.3). In this regard, *binocular* near-eye light field displays have a key advantage: they present accurate binocular disparity and a light field that, under human accommodation, results in near-correct retinal blur. Consider the eye as a simplified camera, comprising a thin lens with an aperture (pupil) diameter a , focused at a distance d_a . A planar object located at a distance d'_o will appear to be blurred by a circle of confusion of width c_a given by

$$c_a = \left(\frac{|d_a - d'_o|}{d_a} \right) a. \quad (14)$$

To emulate retinal blur, a near-eye light field display must approximate this degree of defocus for objects within field.

We reiterate that each lens synthesizes an off-axis perspective projection of the scene (see Figure 1). These projections superimpose on the retina, shifted by an amount determined by the object distance d'_o and the accommodation distance d_a . The minimum number of overlapping views N_v is given by dividing the circle of confusion, evaluated in the lens array plane, by the lens width:

$$N_v = \left\lfloor \frac{c_a}{w_l} \right\rfloor = \left\lfloor \left(\frac{|d_a - d'_o|}{d_a} \right) \left(\frac{a}{w_l} \right) \right\rfloor, \text{ for } d'_o = d_e. \quad (15)$$

As shown in Figure 10, the perceived retinal blur behaves similarly to that observed with *refocused* images produced by light field cameras [Ng et al. 2005]; the approximation becomes more accurate as the number of views N_v increases. Consider the limit as $\{d_o, d_a\} \rightarrow \infty$ (i.e., $\{d_o, d_a\} \gg d_e$). Equation 15 takes the form:

$$\lim_{\{d_o, d_a\} \rightarrow \infty} N_v = \left\lfloor \left(\frac{d_e}{f} \right) \left(\frac{a}{w_e} \right) \right\rfloor, \text{ for } w_l \leq \frac{d_e w_s}{d_e + f} \text{ and } d_l = f, \quad (16)$$

where Equations 6 and 9 give $w_e = (d_e/f)w_l$ for $d_o \rightarrow \infty$. This expression reveals the inverse relationship between spatial resolution and retinal blur fidelity: **the number of overlapping views N_v , approximating retinal blur, is proportional to the ratio of eye relief d_e to the lens focal length f** . In conclusion, magnifier arrays enable thin form factors, by employing shorter focal length lens than allowed with simple magnifiers; yet, HMD designers, as with light field camera engineers, must balance the trade-off between spatial resolution and retinal blur fidelity—a trade-off that is increasingly acceptable if microdisplay pixels continue to shrink.

4 Implementation

4.1 Hardware Implementation

LVT-based Film Prototype: Two near-eye light field displays were implemented: a static film-based prototype and a dynamic OLED-based prototype. As shown in Figure 8 and further described in the supplementary material, a light valve technology (LVT) film recorder was used to develop 3.75×3.75 cm color transparencies at 120 pixels per mm (ppmm). The transparencies were backlit to emulate high-resolution microdisplays. The magnifier array comprised a Fresnel Technologies #630 rectangular plano-convex microlens sheet, with lens focal length $f = 3.3$ mm and lens width $w_l = 1.0$ mm. The microlenses were oriented with the planar surface facing the viewer. The separation between the microlens array and the transparency was manually adjusted to form a virtual image at a distance $d_o \approx 1.0$ m (as assessed by a focused camera). For an eye relief $d_e = 2.5$ cm, the equations in Section 3 provide the following estimates of design parameters: spatial resolution $N_p = 534 \times 534$ pixels, field of view $\alpha = 67 \times 67$ degrees, and eye box width $w_e = 7.6 \times 7.6$ mm. The depth of field extends over the interval $23.2 \leq d'_o < \infty$ cm. For a 4 mm pupil, the retinal blur is approximated by $N_v = 4 \times 4$ views, following Equation 15.

OLED-based HMD Prototype: As shown in Figures 1 and 7, a binocular OLED-based prototype was constructed using components from a Sony HMZ-T1 personal media viewer. The case and magnifying eyepieces were removed, exposing a pair of Sony ECX332A microdisplays connected by ribbon cables to a driver board and a push button controller. Each 15.36×8.64 mm microdisplay has 1280×720 24-bit color pixels (i.e., 83.3 ppmm). Replicating the LVT-based prototype, Fresnel Technologies #630 microlenses were cut and mounted in front of each microdisplay. As shown in Figure 7, a custom head-mount was fabricated using a Dimension 1200es 3D printer. (See Appendix A of the supplementary material for an extended description of the HMD construction.)

The equations in Section 3 provide the following estimates of design parameters for each modified eyepiece: spatial resolution

$N_p = 146 \times 78$ pixels, field of view $\alpha = 29.2 \times 16.0$ degrees, and eye box width $w_e = 7.6 \times 7.6$ mm. The depth of field extends over $30.6 \leq d_o' < \infty$ cm. We emphasize that the OLED- and LVT-based prototypes depict retinal blur with an identical number of views (e.g., $N_v = 4 \times 4$ views for a 4 mm pupil), since they employ the same microlens array. Unlike integral imaging displays viewed at a distance, near-eye conditions interchange conventional spatio-angular resolution trade-offs: increasing lens width w_l (thus increasing lens focal length f to maintain eye box width w_e) *increases* spatial resolution N_p , but decreases views approximating retinal blur N_v , by application of Equations 11 and 16.

The prototype weighs 109 g. In comparison, the HMZ-T1 weighs 420 g. Components contribute as follows: enclosure (65.1 g), driver board and pushbutton controller (16.5 g), and microdisplays (11.8 g each). Each prototype eyepiece is 1.0 cm thick and weighs 16.9 g, with the microlenses contributing only 1.0 g (see Figure 9). In comparison, the HMZ-T1 eyepiece is 3.8 cm thick and weighs 69.4 g. As demonstrated, our design opens the door to significant reductions in HMD weight and form factor: with waist-mounted electronics, only 33.8 g (i.e., a pair of modified eyepieces) must be head-mounted; as illustrated in Figure 1, such a design begins to reflect the form of sunglasses, rather than conventional HMDs.

4.2 Software Implementation

Light Field Ray Tracing: The software implementation addresses two challenges: real-time, stereoscopic light field rendering and robust calibration and correction of mechanical alignment errors and optical aberrations. The LVT- and OLED-based prototypes contain magnifier arrays with 35×35 and 14×8 lenses, respectively. A direct extension of rasterization would require rendering one projection of the 3D scene for each lens, although only for pixels spanning the corresponding elemental image. As an alternative, we modified the NVIDIA OptiX GPU-accelerated ray tracing engine [Parker et al. 2010] to support quad buffering in OpenGL—providing the HDMI 1.4a frame-packed 3D format required by the HMZ-T1. As shown in the supplementary video, frame rates for sample scenes varied from 15–70 Hz using a 3.2 GHz Intel Core i7 workstation with 8 GB of RAM and an NVIDIA Quadro K5000 graphics card.

Supporting Stereoscopic Content: To implement a complete display system, a “backward compatibility” option is required to support existing stereoscopic sources, including movies and video games. We propose the following solution: emulating the appearance of a conventional, planar autostereoscopic display (see Figure 12). For our OpenGL-based implementation, each view is rendered to a texture attached to a frame buffer object (FBO). Following Appendices B and C of the supplementary material, a custom GLSL fragment shader generates elemental images by sampling each view texture, as mapped onto the virtual display plane. As shown in the supplementary “case study” video, this shader allowed *Doom 3 BFG Edition* to be adapted for the HMD prototype.

Calibration Software: During assembly, horizontal and vertical stripes are displayed on the OLEDs. The microlens array is rotated such that the stripes appear aligned to the microdisplay pixel grid. In practice, this procedure achieves accurate rotational alignment, but the lateral displacement must be corrected by translating the rendered images. Similarly, the manufactured focal length and lenslet width may differ from specifications; both of which are manually tuned using test images. Similar to Pamplona et al. [2012], spherical aberrations can be corrected, independently for each eye, by scaling the depth of the rendered scene. Viewers with minimal astigmatism report that, after calibration, the prototype can be viewed comfortably without eyeglasses. These alignment and correction tasks reduce to defining the design parameters in a configuration file. A simple calibration routine, presenting a set of test

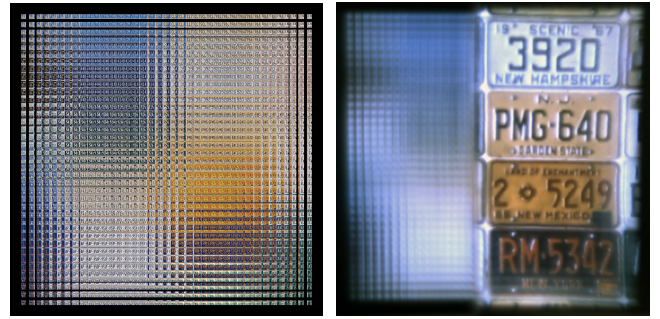


Figure 8: The LVT-based prototype. (Left) The interlaced set of elemental images required to depict a set of license plates separated by 1.0 m from the viewer. (Zoom in to see the detailed microstructure.) (Right) A microlens array is placed over the right half of the developed LVT film. A sharp image is perceived, when viewed through the microlenses, whereas the bare LVT appears defocused. License plates source image courtesy Flickr user “woody1778a”.

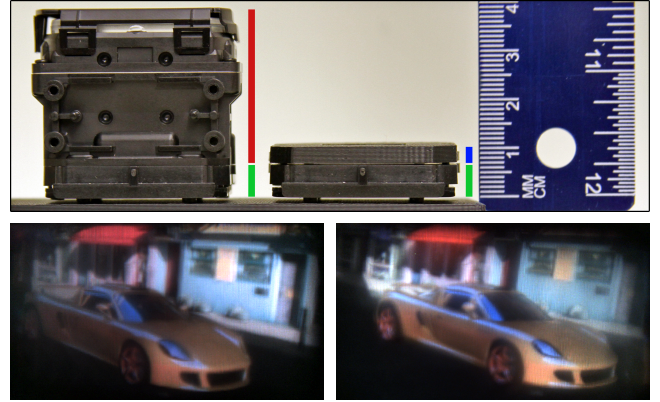


Figure 9: The OLED-based prototype. (Top) A modified eyepiece and a Sony HMZ-T1 eyepiece are compared on the right and left; the ruler illustrates thicknesses of 1.0 cm and 3.8 cm, respectively. The microlens array (length shaded blue) is significantly thinner than the OLED enclosure (shaded green) and the HMZ-T1 magnifying optics (shaded red). (Bottom) A stereoscopic pair of photographs of the binocular HMD prototype. The left-eye and right-eye images are interchanged to facilitate cross-fused stereo viewing.

images including a Snellen chart, allows the user to interactively adjust these parameters. As described in Section 3.1, the user may also tune the interpupillary distance (IPD), by translating the displayed imagery, mitigating the need for mechanical adjustment.

5 Discussion

5.1 Assessment

The performance of the prototypes is illustrated by close-up photographs in Figures 1 and 8–10 and in the supplementary videos. All imagery was captured using a 1600×1200 Point Grey Flea3 camera with a Fujinon 2.8–8 mm varifocal lens supporting a minimum f-number of 1.2 (selected to approximate the human eye).

A central benefit of near-eye light fields displays is to support approximate retinal defocus blur, consistent with convergence of the eyes. A stereoscopic pair is shown in Figure 9, demonstrating the perception of a user wearing the device close to his face, as in Figure 1. The accuracy of retinal imagery is visually assessed in Figure 10. Figure 11 uses the simulation in Figure 10 to quantify the peak signal-to-noise ratio (PSNR) of the retinal im-

ages; this investigates a key issue: are a limited number of overlapping views N_v sufficient to approximate retinal defocus and mitigate accommodation-convergence conflict? Following Shibata et al. [2011], the “zone of comfort” defines comfortable combinations of convergence and accommodation (i.e., the region enclosed by white lines). The prototype achieves a moderate PSNR within this zone, due to “pixelization” artifacts owing to its limited resolution. However, PSNR markedly rises outside this region. As a result, near-eye light field displays enhance retinal blur depiction precisely within the zone where accommodation-convergence occurs. (See Appendix D of the supplementary material for extended analysis.)

5.2 Benefits and Limitations

Higher-resolution Microdisplays: Realizing practical applications will require two key refinements in semiconductor manufacturing: higher-resolution and larger-format microdisplays. Current microdisplays already rival the $8.3\text{ }\mu\text{m}$ pixel pitch of the LVT prototype. The Sony ECX332A in the HMD prototype has a $12.0\text{ }\mu\text{m}$ pitch. OLEDs with smaller pitches include the Sony ECX331A ($9.9\text{ }\mu\text{m}$) and eMagin WUXGA ($9.6\text{ }\mu\text{m}$). The Citizen Miyota LCoS ($7.8\text{ }\mu\text{m}$) and Kopin 152K LCD ($7.0\text{ }\mu\text{m}$) even exceed the LVT pitch. Market trends are driving such high-resolution microdisplays, particularly the adoption of “4K” resolutions, enabling the next generation of viewfinders, projectors, and consumer HMDs.

Larger-Format Microdisplays: Today’s microdisplays measure less than 25 mm diagonally, limiting the prototype field of view. Tiling microdisplays overcomes this limitation, at the cost of reducing the eye box width (i.e., to hide inactive regions between tiles). Since microdisplays rely on semiconductor manufacturing, their dimensions are constrained by the maximum photolithographic reticle area (currently approximately 550 mm^2 , corresponding to APS-H image sensors). However, medium-format digital cameras reveal a path forward: multiple, laterally-shifted reticles are aligned between exposures to achieve active areas approaching $2,000\text{ mm}^2$.

Manufacturing yield for large-format microdisplays may similarly be improved by compensating for defects (i.e., “stuck” or “dead” pixels). While redundancy in the elemental image array is the origin of resolution loss, it also provides a means to correct defects. A defective pixel corresponds to an emitted ray passing through a virtual point—a point that is replicated in many other elemental images (e.g., multiple bird beak copies in Figure 1); thus, the intensities of the corresponding ray bundle can be adjusted to compensate. Even in the absence of defects, redundancy similarly allows for increased color depth. (See Appendix E of the supplementary material for preliminary results using a tomographic correction framework.)

Diffraction Limit: Pixel pitches cannot reduce below the diffraction limit imposed by individual lenses. Following Goodman [2004], far-field diffraction by a square lens, of width w_l and with microdisplay separation d_l , limits the pitch p to $\lambda d_l / w_l$. For our microlens array, the pitch is limited to $2.6\text{ }\mu\text{m}$ for “deep red” illumination ($\lambda = 780\text{ nm}$). Less conservatively, pitch could be decreased to $1.8\text{ }\mu\text{m}$ and $1.3\text{ }\mu\text{m}$ for green (550 nm) and blue (390 nm) illumination, respectively. Averaged over the visible spectrum, the HMD prototype resolution can increase by roughly a factor of six to 876×468 pixels. In this circumstance, the angular resolution, at 30 pixels per degree (ppd), is competitive with the Sony HMZ-T1 (25 ppd) and the Oculus Rift (10 ppd). Further gains could be realized with wider lenses, at the cost of decreased retinal blur accuracy.

Additional Limitations: Our microlens-based design shares the limitations of other integral imaging displays, including the creation of a periodic eye box. Collimating materials would eliminate this repetition. Structured illumination could be applied, similar to Levoy et al. [2009], to more accurately calibrate the mapping from

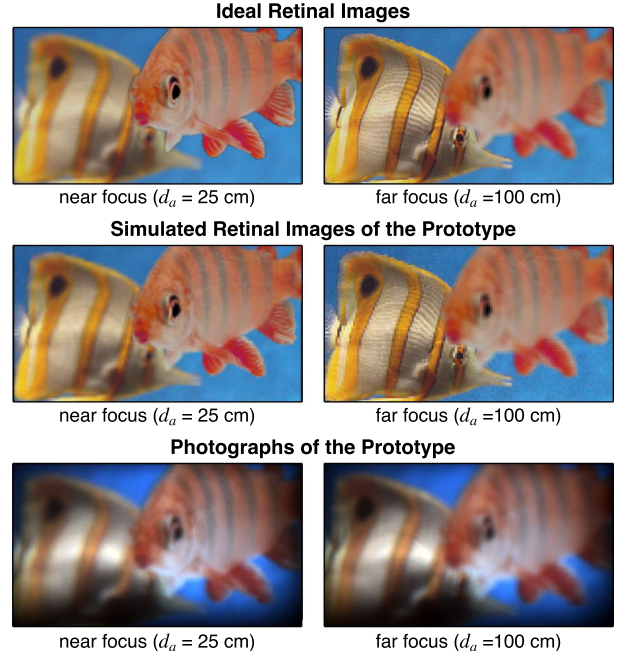


Figure 10: Approximating retinal blur. (Top) Ideal retinal images are evaluated using Equation 14. The fish on the right and left are located distances of 25 cm and 100 cm away, respectively. (Middle) A ray tracing model, implemented in Matlab, simulates the retinal images for the OLED-based prototype in Section 4. (Bottom) Photographs of the prototype are in close agreement. Following Equation 15, retinal defocus blur is approximated by averaging overlapping views from lenses spanning the circle of confusion. Butterfly-fish source image courtesy Richard Luney.

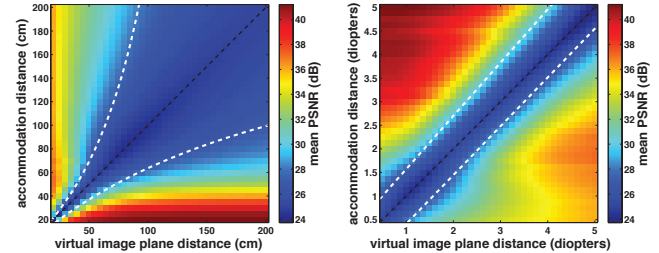


Figure 11: Approximating retinal defocus blur using near-eye light field displays. The PSNR is tabulated as a function of virtual image distance and accommodation distance, expressed in centimeters (left) and diopters (right). The dashed white lines denote the boundary of the “zone of comfort” estimated by Shibata et al. [2011].

microdisplay pixels to rays of the emitted light field. We observe that such generalized sampling patterns could be added to both our ray tracing solution and our backward-compatible shader program.

5.3 Future Work

Our choice of microlens array was constrained by off-the-shelf offerings, given the prohibitive costs of custom tooling. As a result, the prototypes have narrower eye boxes than desired. However, with the addition of eye tracking, narrower eye boxes will yield commensurate gains in resolution. Papas et al. [2012] describe microlens fabrication by engraving and 3D printing; applying similar methods is a promising direction for future work. Such approaches may allow fabrication of curved arrays for use with flexible OLEDs, mitigating artifacts at steep viewing angles. Anti-reflection coatings may further reduce artifacts. Another avenue of research is to lever-

age advances made by the microlens array imaging community to further refine fabrication, alignment, and calibration. While perceived resolution is constrained by the diffraction limit imposed by each microlens, there is an opportunity to similarly apply diffractive optical elements [Pastoor and Wöpking 1997; Bunkenburg and Droeßler 1998] within near-eye light field displays.

Engineering practical near-eye light field displays will require producing binocular light field content, necessitating methods to capture live action and to render synthetic scenes. We anticipate the use of binocular light field cameras, in concert with our displays, to create immersive telepresence systems. While general ray tracing is sufficient for our proof-of-concept demonstrations, accelerated methods, such as the backward-compatible shader program, are needed to mitigate computational overhead. Similar to Lehtinen et al. [2011], exploiting structure in the light field may minimize overhead for general 3D scenes. As with any display system, efficient anti-aliasing algorithms must also be developed, drawing upon prior work on light field anti-aliasing [Zwicker et al. 2006].

6 Conclusion

Near-eye displays are poised to enter the consumer market. However, emerging devices present one of two restrictive solutions: either narrow-field-of-view displays, located in the periphery of a viewer's visual field, or bulky designs held in place with tight straps. These compromises are necessary to achieve lightweight, eyeglasses-like form factors, with the former, or to obtain wide-field-of-view, immersive experiences, with the latter. Commercial near-eye displays have not yet met these demands with thin, lightweight designs. The microlens-based display system we demonstrate is aimed at enabling wide-field-of-view, immersive experiences with compact, comfortable eyewear—offering a new path to practical head-mounted displays that trades spatial resolution for significant improvements in field of view, weight, and form factor.

Acknowledgements

We thank the reviewers for their helpful feedback. We also thank Frank Fox and Gerrit Slavenburg, from NVIDIA Consumer Electronics Engineering, for motivating the authors to pursue the topic of near-eye light field displays. Similarly, we recognize the support of the NVIDIA Industrial Design team, particularly Don Miller, who assisted in the fabrication of the prototype HMD enclosure.

References

- AKELEY, K., WATT, S. J., GIRSHICK, A. R., AND BANKS, M. S. 2004. A stereo display prototype with multiple focal distances. *ACM Trans. Graph.* 23, 804–813.
- ANDERSON, R. H. 1979. Close-up imaging of documents and displays with lens arrays. *Applied Optics* 18, 4, 477–484.
- BUNKENBURG, J., AND DROESSLER, T. A. 1998. Innovative diffractive eyepiece for a helmet-mounted display. In *Proc. SPIE*, vol. 3430, 41–49.
- DODGSON, N. A. 2002. Analysis of the viewing zone of multi-view autostereoscopic displays. In *SPIE SD&A XIII*, 254–265.
- GOODMAN, J. 2004. *Introduction to Fourier Optics*. Roberts and Company Publishers.
- GOTODA, H. 2010. A multilayer liquid crystal display for autostereoscopic 3D viewing. In *SPIE SD&A XXI*, vol. 7524, 1–8.
- HELD, R. T., COOPER, E. A., AND BANKS, M. S. 2012. Blur and disparity are complementary cues to depth. *Current Biology* 22, 5, 426–431.
- HOBBS, P. C. D. 2009. *Building Electro-Optical Systems: Making It all Work*. John Wiley & Sons.
- HOLROYD, M., BARAN, I., LAWRENCE, J., AND MATSIK, W. 2011. Computing and fabricating multilayer models. *ACM Trans. Graph.* 30, 6, 187:1–187:8.
- HUTLEY, M. C., HUNT, R., STEVENS, R. F., AND SAVANDER, P. 1994. The moiré magnifier. *Pure and Applied Optics* 3, 2.
- IVES, F. E., 1903. Parallax stereogram and process of making same. United States Patent 725,567.
- JIN, F., JANG, J.-S., AND JAVIDI, B. 2004. Effects of device resolution on three-dimensional integral imaging. *Optics Letters* 29, 12, 1345–1347.
- KIM, Y., KIM, J., KANG, J.-M., JUNG, J.-H., CHOI, H., AND LEE, B. 2007. Point light source integral imaging with improved resolution and viewing angle by the use of electrically movable pinhole array. *Optics Express* 15, 26, 18253–18267.
- KRESS, B., AND STARNER, T. 2013. A review of head-mounted displays (HMD) technologies and applications for consumer electronics. In *Proc. SPIE*, vol. 8720.
- LEHTINEN, J., AILA, T., CHEN, J., LAINE, S., AND DURAND, F. 2011. Temporal light field reconstruction for rendering distribution effects. *ACM Trans. Graph.* 30, 4, 55:1–55:12.
- LEVOY, M., ZHANG, Z., AND McDOWALL, I. 2009. Recording and controlling the 4D light field in a microscope using microlens arrays. *Journal of Microscopy* 235, 2, 144–162.
- LIPPmann, G. 1908. Épreuves réversibles donnant la sensation du relief. *Journal of Physics* 7, 4, 821–825.
- LIU, S., HUA, H., AND CHENG, D. 2010. A novel prototype for an optical see-through head-mounted display with addressable focus cues. *IEEE Trans. Visualization and Computer Graphics* 16, 3, 381–393.
- LOVE, G. D., HOFFMAN, D. M., HANDS, P. J., GAO, J., KIRBY, A. K., AND BANKS, M. S. 2009. High-speed switchable lens enables the development of a volumetric stereoscopic display. *Optics Express* 17, 18, 15716–15725.
- MANN, S. 2012. Through the glass, lightly. *IEEE Technology and Society Magazine* 31, 3, 10–14.
- MASSOF, R. W., BROWN, L. G., SHAPIRO, M. D., BARNETT, G. D., BAKER, F. H., AND KUROSAWA, F. 2003. Full-field high-resolution binocular HMD. *SID Digest* 34, 1, 1145–1147.
- NG, R., LEVOY, M., BRÉDIF, M., DUVAL, G., HOROWITZ, M., AND HANRAHAN, P. 2005. Light field photography with a handheld plenoptic camera. Tech. Rep. CTSR 2005-02, Stanford.
- OLSON, J., KRUM, D., SUMA, E., AND BOLAS, M. 2011. A design for a smartphone-based head mounted display. In *IEEE Virtual Reality*, 233–234.
- PAMPLONA, V. F., MOHAN, A., OLIVEIRA, M. M., AND RASKAR, R. 2010. NETRA: interactive display for estimating refractive errors and focal range. *ACM Trans. Graph.* 29.
- PAMPLONA, V. F., OLIVEIRA, M. M., ALIAGA, D. G., AND RASKAR, R. 2012. Tailored displays to compensate for visual aberrations. *ACM Trans. Graph.* 31, 4, 81:1–81:12.

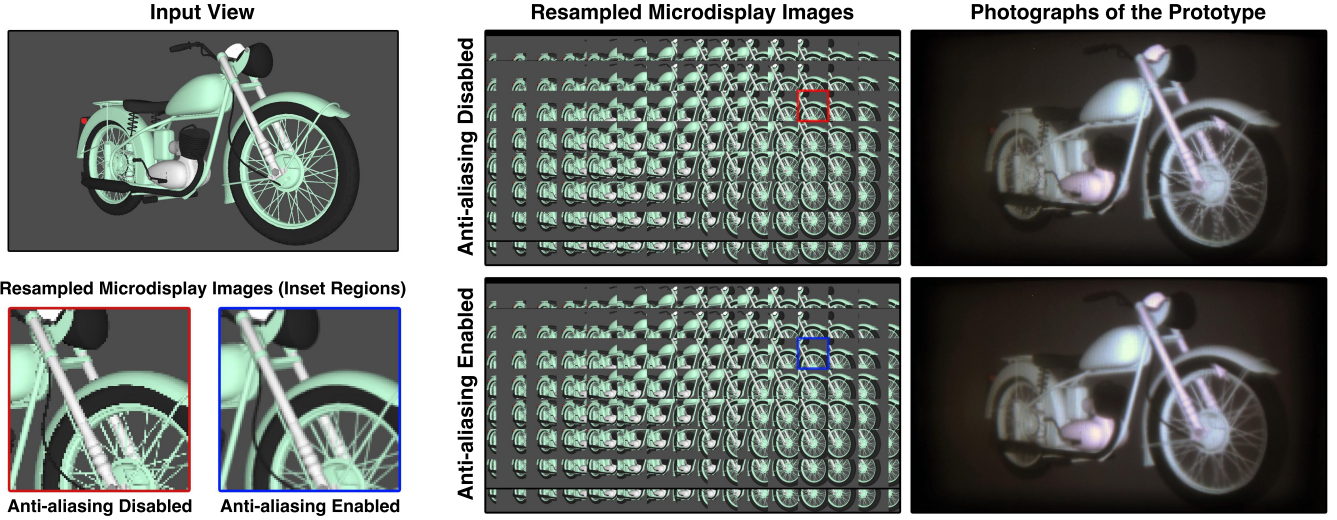


Figure 12: Supporting stereoscopic content. As described in Section 4.2, a custom fragment shader program was used to resample stereoscopic image pairs for presentation using the binocular near-eye light field display prototype. (Top Left) A right-eye view rendered using an OpenGL-based model viewer application. (Middle) Resampled microdisplay images. (Right) Corresponding photographs of the prototype near-eye light field display. (Bottom Left) Inset regions demonstrate the benefit of applying an additional fragment shader program implementing full-scene anti-aliasing (FSAA). See Appendices B and C of the supplementary material for additional implementation details.

PAPAS, M., HOUIT, T., NOWROUZEZAHRAI, D., GROSS, M., AND JAROSZ, W. 2012. The magic lens: refractive steganography. *ACM Trans. Graph.* 31, 6, 186:1–186:10.

PARKER, S. G., ET AL. 2010. OptiX: a general purpose ray tracing engine. *ACM Trans. Graph.* 29, 4, 66:1–66:13.

PASTOOR, S., AND WÖPKING, M. 1997. 3-D displays: A review of current technologies. *Displays* 17, 2, 100–110.

PERLIN, K., PAXIA, S., AND KOLLIN, J. S. 2000. An autostereoscopic display. In *ACM SIGGRAPH*, 319–326.

ROLLAND, J., AND HUA, H. 2005. Head-mounted display systems. *Encyclopedia of Optical Engineering*, 1–13.

ROLLAND, J. P., KRUEGER, M. W., AND GOON, A. 2000. Multifocal planes head-mounted displays. *Applied Optics* 39, 19.

SHAOULOV, V., MARTINS, R., AND ROLLAND, J. P. 2004. Compact microlenslet-array-based magnifier. *Optics Letters* 29, 7.

SHIBATA, T., KIM, J., HOFFMAN, D. M., AND BANKS, M. S. 2011. The zone of comfort: Predicting visual discomfort with stereo displays. *Journal of Vision* 11, 8.

SUTHERLAND, I. E. 1968. A head-mounted three dimensional display. In *AFIPS Fall Joint Computer Conference*, 757–764.

TAKAKI, Y. 2006. High-density directional display for generating natural three-dimensional images. *Proceedings of the IEEE* 94.

UREY, H., AND POWELL, K. D. 2005. Microlens-array-based exit-pupil expander for full-color displays. *Applied Optics* 44.

WANDELL, B. A. 1995. *Foundations of Vision*. Sinauer Associates.

WETZSTEIN, G., LANMAN, D., HIRSCH, M., AND RASKAR, R. 2012. Tensor displays: compressive light field synthesis using multilayer displays with directional backlighting. *ACM Trans. Graph.* 31, 4, 80:1–80:11.

ZWICKER, M., MATUSIK, W., DURAND, F., AND PFISTER, H. 2006. Antialiasing for automultiscopic 3D displays. In *EGSR*.

A Bounding Thin-Lens Magnifier Thickness

This appendix presents a lower bound on the thickness of any HMD employing a simple magnifier (under the thin lens approximation). Building on the analysis in Section 3.1, we consider the circumstance for which the virtual image plane is placed at “optical infinity”, such that $d_o \rightarrow \infty$ (equivalent to the condition $d_o \gg d_e$). By Equation 1, the lens separation d_l equals the lens focal length f . The eye box width w_e is given by Equation 5:

$$\lim_{d_o \rightarrow \infty} w_e = \left| w_l - \left(\frac{d_e}{f} \right) w_s \right|, \text{ for } d_l = f. \quad (17)$$

For display-limited magnifiers, inspection of Figure 3 and Equation 17 provides the constraint that $w_l \geq (d_e/f)w_s$. In addition, the f-number N is defined as the ratio of the lens focal length f to the diameter w_l (i.e., $f = Nw_l$). Combining these two constraints yields the following quadratic inequality for the focal length f .

$$f^2 - Nw_e f - Nd_e w_s \geq 0, \text{ for } f \geq Nw_l \quad (18)$$

We conclude that any HMD constructed using a display-limited magnifier must have a lens focal length f satisfying

$$f \geq \frac{Nw_e + \sqrt{N^2 w_e^2 + 4Nd_e w_s}}{2} \geq \sqrt{Nd_e w_s}. \quad (19)$$

Equation 19 establishes the fundamental form factor limitation of HMDs using simple magnifiers. For example, consider the design parameters for the prototype in Section 4: microdisplay width $w_s = 15.36$ mm, eye box width $w_e = 10$ mm, and eye relief $d_e = 14$ mm. In practice, low f-numbers are feasible, but difficult to achieve without multiple elements, high indices of refraction, or aspheric surfaces [Hobbs 2009]. Assuming a minimum f-number of 1.0, the lens focal length f , and therefore the HMD itself, must have a thickness exceeding 20.5 mm (i.e., much thicker than eyeglasses). While commercial non-pupil-forming HMDs use compound sets of thick lenses, this constraint underscores the need for alternative architectures—such as near-eye light field displays—to achieve target resolutions and fields of view with more comfortable form factors.